# X-ray transparent microfluidic chips for high-throughput screening and optimization of *in meso* membrane protein crystallization

Jeremy M. Schieferstein, Ashtamurthy S. Pawate, (iD) Chang Sun, et al.

View Online          Export Citation          CrossMark

## ARTICLES YOU MAY BE INTERESTED IN

# X-ray transparent microfluidic chips for high-throughput screening and optimization of *in meso* membrane protein crystallization

Jeremy M. Schieferstein,[1] Ashtamurthy S. Pawate,[1] Chang Sun,[2] Frank Wan,[1] Paige N. Sheraden,[2] Jana Broecker,[3] Oliver P. Ernst,[3,4] Robert B. Gennis,[2] and Paul J. A. Kenis[1]

[1]*Department of Chemical and Biomolecular Engineering, University of Illinois at Urbana-Champaign, Urbana, Illinois 61801, USA*
[2]*Department of Biochemistry, University of Illinois at Urbana-Champaign, Urbana, Illinois 61801, USA*
[3]*Department of Biochemistry, University of Toronto, Toronto, Ontario M5S IA8, Canada*
[4]*Department of Molecular Genetics, University of Toronto, Toronto, Ontario M5S IA8, Canada*

Elucidating and clarifying the function of membrane proteins ultimately requires atomic resolution structures as determined most commonly by X-ray crystallography. Many high impact membrane protein structures have resulted from advanced techniques such as *in meso* crystallization that present technical difficulties for the set-up and scale-out of high-throughput crystallization experiments. In prior work, we designed a novel, low-throughput X-ray transparent microfluidic device that automated the mixing of protein and lipid by diffusion for *in meso* crystallization trials. Here, we report X-ray transparent microfluidic devices for high-throughput crystallization screening and optimization that overcome the limitations of scale and demonstrate their application to the crystallization of several membrane proteins. Two complementary chips are presented: (1) a high-throughput screening chip to test 192 crystallization conditions in parallel using as little as 8 nl of membrane protein per well and (2) a crystallization optimization chip to rapidly optimize preliminary crystallization hits through fine-gradient re-screening. We screened three membrane proteins for new *in meso* crystallization conditions, identifying several preliminary hits that we tested for X-ray diffraction quality. Further, we identified and optimized the crystallization condition for a photosynthetic reaction center mutant and solved its structure to a resolution of 3.5 Å. *Published by AIP Publishing.* [http://dx.doi.org/10.1063/1.4981818]

## I. INTRODUCTION

Fundamental understanding of membrane protein function requires atomic resolution structures obtained most commonly by X-ray crystallography.[1] As membrane proteins play key physiological roles linked to health and disease (accounting for >60% of all drug targets), crystal structures of membrane proteins are of paramount importance for structure-based rational drug design.[2,3] Crystallization itself, however, remains one of the largest bottlenecks in resolving atomic resolution structures. Membrane proteins are inherently amphiphilic, which limits their solubility and stability in aqueous solutions and in turn can reduce crystallization success rates.[4] Crystallization in lipidic mesophases (*in meso* crystallization) occurs in a crystallization-compatible cell membrane-mimetic environment and has resulted in increased success rates for membrane protein crystallization.[5] While the method requires a high level of technical expertise, the effectiveness and improved success rates of *in meso* crystallization have made it a staple in structural biology, leading to over 200 atomic resolution structures in the past two

decades, most notably of several previously intractable G-protein coupled receptor (GPCR) and the $\beta_2$-adrenergic receptor-$G_s$ protein complex.[6,7]

A multi-component precipitant mixture of salts and other additives triggers the crystallization of membrane proteins *in meso*.[8] Unfortunately, protein crystallization conditions cannot be determined *a priori*, thus requiring extensive screening of hundreds to thousands of potential precipitant mixtures to find one that yields diffracting crystals.[9,10] To obtain crystals that diffract to atomic resolution, optimization by fine-gradient re-screening of crystallization conditions[11,12] and precipitants[13] must often be done. The *in meso* method is tedious: the preparation of high viscosity protein-laden lipidic mesophases requires specialized tools and manual expertise for precise handling and dispensing, which complicates the set-up and repeatability of high-throughput screens and optimization at nanoliter volumes. Further difficulties arise after crystallization when crystals are usually physically transferred by the operator to a synchrotron-compatible holder and then flash frozen for X-ray analysis, a process which may damage the crystal and decrease the quality of X-ray diffraction data.[14,15]

For traditional *in meso* crystallization experiments, several microliters of protein and lipid are mixed in coupled-syringes to form a highly viscous protein-laden mesophase. A protein-to-lipid ratio of 2:3 is typically selected from the temperature-composition diagram of lipid in water to form a stable cubic mesophase at room temperature for crystallization. In multicomponent crystallization mixtures of lipid, protein, salts, detergents, and other additives, the mesophase behavior can change and ratios other than 2:3 may be ideal for stable cubic phases and crystallization, and in extreme cases, unexpected phases will form, such as sponge phases.[16–18] In a few reports, other mixing ratios, formulations, and variant *in meso* methods have demonstrated successful crystallization: a reaction center was crystallized by overlaying protein over lipid for passive mixing by diffusion at a 2:1 protein-to-lipid ratio;[19] a separate effort demonstrated passive mixing followed by controlled dehydration of the mesophase for crystallization.[20] These methods showed that (1) crystallization-compatible mesophases can be formed reliably by passive mixing rather than coupled-syringe mixing and (2) crystallization success can be affected by mesophase formulation and mesophase/protein mixing ratio, probably by influencing the amounts of protein and detergent incorporated in the same volume of mesophase.

State-of-the-art methods for high-throughput screening and optimization of *in meso* crystallization often rely on robots to dispense mesophase boluses.[21,22] The most common types of well-plates for crystallization with robots are hermetically sealed glass-sandwich crystallization plates. Glass-sandwich plates are incompatible with *in situ* X-ray analysis, and the high viscosity of the mesophase plus the need to cut through the glass-sandwich plate to gain access to each crystallization well require manual expertise to harvest the crystals and are time-consuming.[21,23] Recent reports demonstrate *in meso in situ* X-ray crystallography by replacing glass plates with thin layers of either cyclic olefin copolymer (COC)[24] or Mylar,[25] both materials with low background scattering and high transmission for X-rays. While a significant step forward for high-throughput *in meso* screening, the use of these X-ray transparent plates still relies in many cases on dispensing robots which perform crystallization in mesophases as small as 30–40 nl.

As an alternative approach, several microfluidic devices have successfully addressed formulation of *in meso* crystallization trials. The first microfluidic devices for *in meso* crystallization formulated mesophases by passive mixing in droplets[26] or chaotic mixing in microchambers.[27] Both of these microfluidic approaches successfully yielded diffraction quality crystals, but the chips were an additional barrier to solving crystal structures as neither approach facilitated the process of crystal harvesting and X-ray analysis. To overcome this hurdle, a set of design principles were developed to build thin X-ray transparent microfluidic devices for crystal growth and *in situ* X-ray analysis.[28,29] For X-ray diffraction experiments, the entire chip was mounted in front of an X-ray source, and the resulting crystal structures had very good resolution and mosaicity, two parameters that often suffer as a result of crystal harvesting. An X-ray transparent device for *in meso* crystallization for passive mixing of protein and lipid was developed and validated by crystallizing and solving a high-resolution structure of a membrane protein.[30] Formulation was automated by loading protein directly on-top of lipid to create a large, open-interface for mixing by

diffusion; the subsequent addition of a precipitant into a connected adjacent well triggered crystallization. The application of these *in meso* devices as all-in-one mesophase formulation, crystallization, and X-ray diffraction tools for routine experiments, such as screening and optimization, is limited by scale (50–70 nl mesophases in each well, 12 well arrays).

Building on these prior efforts, this work overcomes the scaling limitations of X-ray transparent *in meso* crystallization devices and demonstrates their applicability in routine crystallization experiments, specifically high-throughput condition screening and optimization. First, the limitations of scale-down were addressed to efficiently utilize precious membrane protein solution. To achieve this, a capillary-valve strategy was developed to deliver as little as 8 nl of membrane protein (to form 13 nl of protein-laden mesophase) into open-interface crystallization wells. Second, the limitations of scale-out were addressed by designing densely packed microfluidic arrays to screen up to 192 potential crystallization conditions and combinatorial microfluidic arrays to generate 16 fine-gradient condition variants to optimize crystallization conditions. To validate the effectiveness of these microfluidic devices for routine crystallization experiments, they were used: (1) as high-throughput screening tools to identify new crystallization hits of three membrane proteins with limited or no structural data: quinol-dependent nitric oxide reductase, cytochrome $bo_3$ oxidase, and the LM-dimer of the photosynthetic reaction center and (2) as crystallization optimization tools to increase the size and diffraction quality of crystals of a reaction center mutant, L223SW, from which the structure was solved to a resolution of 3.5 Å.

## II. MATERIALS AND METHODS

### A. Chemicals

For the experiments described here, we used screening kits (Cubic Screen 96-well screening kit from Emerald Biosystems, now distributed as Wizard Cubic Screen from Molecular Dimensions, Altamonte Springs, FL), monoolein (1-Oleoyl-*rac*-glycerol) and cholesterol (Sigma–Aldrich, St. Louis, MO), polydimethylsiloxane (PDMS) (RTV-615 from Momentive Performance Adhesives, Waterford, NY), negative photoresists (SU-8 25 and SU-8 2050 from MicroChem Corporation, Newton, MA), cyclic olefin copolymer films (COC) (Grade 6013, 2 mil from TOPAS Advanced Polymers, Florence, KY), silanizing agent (tridecafluoro-1,1,2,2-tetrahydrooctyl)trichlorosilane from Gelest, Inc., Morrisville, PA), and epoxy (Conapoxy FR 1080 from Cytec Industries, Woodland Park, NJ). All other salts, precipitants, and solvents were purchased from Sigma–Aldrich and Hampton Research and used without further purification.

### B. Protein sample preparation

#### 1. Bacterial photosynthetic reaction center/LM dimmer

Site-directed mutagenesis was first carried out in the pUCLHRC plasmid as described previously.[31] pUCLHRC is based on the commonly used cloning vector pUC19 and has the photosynthetic *puh* and *puf* operons integrated as a 5 kb *Bam*HI/*Eco*RI fragment. After verifying the mutation with DNA sequencing, the mutated fragment was cleaved and incorporated to vector pATP19P,[32] which, unlike pUC19 based plasmids, can be maintained in *Rhodobacter sphaeroides*. This mutated plasmid was then transferred to the *R. sphaeroides* strain ΔLHRC (knock-out of reaction center and both light harvesting complexes) via conjugation. Transformed *R. sphaeroides* was cultured in Sistrom medium supplemented with 0.5% yeast extract. Expression of the photosynthetic reaction center was induced automatically at high cell density under low oxygen tension. The purification of the mutant photosynthetic reaction center follows the same protocol for the wild type.[33] Starting with the purified bacterial photosynthetic reaction center which contains three subunits, the LM dimer core complex was prepared by precipitating the H subunit in the presence of lithium perchlorate and ethanol.[34] Extensive dialysis against 10 mM Tris, 0.03% LDAO (N,N-dimethyldodecylamine N-oxide) pH 8 was then carried out to remove these chaotropic agents.

### 2. Cytochrome bo₃ ubiquinol:oxygen oxidoreductase

Wild type cytochrome $bo_3$ oxidase was overexpressed by IPTG (isopropyl $\beta$-D-1-thiogalactopyranoside) induction in *E. coli* strain C43(DE3) transformed with plasmid pETcyo. Bacteria were cultured in M63 minimal medium at 37 °C as previously reported.[35] When the cell density reached an $OD_{600}$ of ~0.6, 0.5 mM IPTG was added to the culture. After 4–6 h of induction to allow protein expression, cells were harvested by centrifugation at 5000 $g$ for 20 min at 4 °C. Cells were then disrupted with a French press. After 10 min of low speed spin at 5000 $g$ to remove cell debris, the cytoplasmic membrane was pelleted at 180 000 $g$ for 4 h at 4 °C. The membrane was then resuspended in 50 mM potassium phosphate pH 8 and solubilized with 1% DDM (*n*-dodecyl $\beta$-D-maltoside), followed by 1 h centrifugation at 180 000 $g$ at 4 °C to remove insoluble membrane fractions. The supernatant containing $bo_3$ oxidase in DDM micelles was loaded onto a Nickel-nitrilotriacetic acid (Ni-NTA) affinity column. After washing with 5 column volumes of 10 mM imidazole, cytochrome $bo_3$ oxidase was eluted with 50 mM imidazole. Extensive dialysis in either 50 mM potassium phosphate, 0.05% DDM or 20 mM Tris-HCl, 0.7% *n*-octyl-$\beta$-D-glucoside (OG) was performed to remove imidazole.

### 3. Quinol nitric oxide reductase (qNOR) preparation

The 2200 base pair qNOR gene from *Peresephonella marina* was amplified from genomic DNA using Polymerase chain reaction (PCR), cloned into the plasmid pET-22b (Novagen), and overexpressed by IPTG induction in *E. coli* strain C43(DE3). Bacteria were cultured in LB media at 37 °C while shaking at 200 rpm. Once the cultures reached an $OD_{600}$ of 0.7, 1 mM IPTG was added to the culture. Cells were harvested after 4 h of induction by centrifugation at 5000 $g$ for 10 min at 4 °C and broken by passing the cell suspension through a Microfluidizer three to four times at a pressure of 80 000 psi. The membrane fraction was collected by centrifugation of the disrupted cell membranes at 180 000 $g$ for 4 h at 4 °C. Isolated membranes were resuspended in buffer containing 100 mM Tris-HCl pH 8 and 100 mM NaCl and solubilized with 1% DDM. The insolubilized membrane was pelleted by a 30 min centrifugation at 180 000 $g$. The supernatant containing qNOR was applied to a Ni-NTA affinity column. The resin was washed in the buffer containing 50 mM imidazole and 0.05% DDM, and then, the protein was eluted in the buffer containing 100 mM imidazole and 0.05% DDM. The protein was concentrated using 100 kDa molecular weight cutoff centrifugal filter units (Millipore) and dialyzed against 100 mM Tris-HCl pH 8, 100 mM NaCl, 0.05% DDM, and 10% glycerol.

For all proteins, small aliquots of the protein sample were flash-frozen in liquid nitrogen and stored at –80 °C until use.

## C. Fabrication of microfluidic chips

Microfluidic chips were fabricated using a strategy adapted from previous work.[30] For a full description, see supplementary material. Briefly, patterned COC substrate layers were fabricated by hot embossing 50 $\mu$m thick sheets of COC with a high temperature epoxy master mold in a laminating press (Carver). Photoresist-on-silicon master molds were fabricated by photolithography using transparency photomasks (Figure S1 (supplementary material)). Polydimethylsiloxane (PDMS), an elastomeric thermoset, was spin-coated on photoresist-on-silicon master molds to fabricate thin, patterned PDMS fluid and control layers by soft lithography. The chip layers were assembled through a combination of irreversible and reversible bonds. A blank COC layer was irreversibly bonded to the PDMS control layer by activating the surfaces with an atmospheric plasma treatment (Harrick) and then bringing them into direct contact. This COC–PDMS control layer was then irreversibly bonded to the PDMS fluid layer by a thermal bonding[36] to form a COC–PDMS–PDMS three-layer assembly (TLA). Prior to crystallization experiments, the compartments in the patterned COC substrate layer were filled with lipid. The crystallization wells in the TLA were aligned to the lipid compartments and reversibly bonded by surface adhesion to complete the construction of the chip. Vacuum interconnects were fabricated from PDMS blocks attached to Polytetrafluoroethylene (PTFE) tubing to facilitate vacuum actuation.

## D. Characterization

### 1. Room-temperature single crystal X-ray diffraction

X-ray diffraction data were collected at APS (Advanced Photon Source) synchrotron, Argonne National Laboratory, specifically beamlines 21-ID-F, LS-CAT (Life Sciences Collaborative Access Team) and 23-ID-B GM/CA (General Medical Sciences and Cancer Institutes Structural Biology Facility). In-line microscopes aided in focusing on crystallization wells and centering on crystals. At 21-ID-F, a $20 \times 20$-$\mu$m microbeam with a wavelength of 0.9795 Å was used, and data were collected in $0.5-1°$ steps with $1-2$ s exposures and sample-to-detector distance between 200 and 500 mm with a MARmosaic 300 detector. At 23-ID-B, data were collected in $0.2-0.4°$ steps with $0.2-0.4$ s exposures and a sample-to-detector distance between 400 and 500 mm with a Pilatus 6 M detector. All data were collected at room temperature, and an on-chip serial crystallography approach was utilized to mitigate the effect of radiation damage as demonstrated in prior work.[30]

### 2. Data reduction and structure determination for L223SW

From the 50 crystals of L223SW mutant, X-ray data from 19 crystals that diffracted to a maximum of 3.2 Å were used for structure determination. HKL2000 software was used for indexing, refinement, integration, and scaling multiple data sets together (HKL Research Inc.).[37] Molecular replacement was performed with Phaser using PDB structure 4TQQ as a model.[30] Structure phasing, building, and refinement were done using the Phenix suite of programs.[38] Ligands bound to the structure were identified in the electron density and built into the final model. Electron density maps were displayed and compared using PyMOL.

### 3. Flash-induced optical spectroscopy

Flash-induced optical spectroscopy was carried out with an in-house designed apparatus. The saturating excitation light pulse, which initiates electron transfer within the photosynthetic reaction center, comes from a Xenon flash lamp controlled by a LabJack U3-LV via TTL signal. The continuous measuring beam from a 12 V tungsten lamp first goes through a Bausch & Lomb monochromator and then passes through the sample cuvette. The transmitted fraction was measured with a photomultiplier as voltage. This signal was recorded by a PicoScope (Model 4424) as a function of delay after the excitation pulse and converted into absorbance using value prior to the excitation pulse as a reference.

## III. RESULTS AND DISCUSSION

### A. Design of a microfluidic well for in meso crystallization

The design goal was to automate the sequential mixing of three components—protein, lipid, and precipitant—in a compact and modular well for scale-out into microfluidic arrays (Figure 1(b)). Individual wells for formulation of *in meso* crystallization trials rely on passive mixing, as demonstrated in prior work.[30] In a microfluidic well, protein solution was layered on top of dry lipid in the chip's substrate layer (Figures 1(a) and 1(c)) for passive formulation of a protein-laden mesophase by mixing across a large lipid-protein interface. After protein-lipid mixing, the protein-laden mesophase becomes very viscous and remains immobile. During mixing, a concentration gradient may form into the $25\,\mu$m depth of the lipid layer, although this effect is difficult to visually observe with light microscopy. Next, a precipitant solution was filled in the other half of the well. The two half-wells (protein/lipid and precipitant) meet in a $75\,\mu$m-wide "S"-shaped channel where mixing of the protein-depleted solution and precipitant occurs by diffusion across a liquid–liquid interface. As the precipitant mixes with the protein-depleted solution, it begins to diffuse into the protein-laden mesophase to trigger crystallization. While mixing of the precipitant into the mesophase is expected to be complete within a few
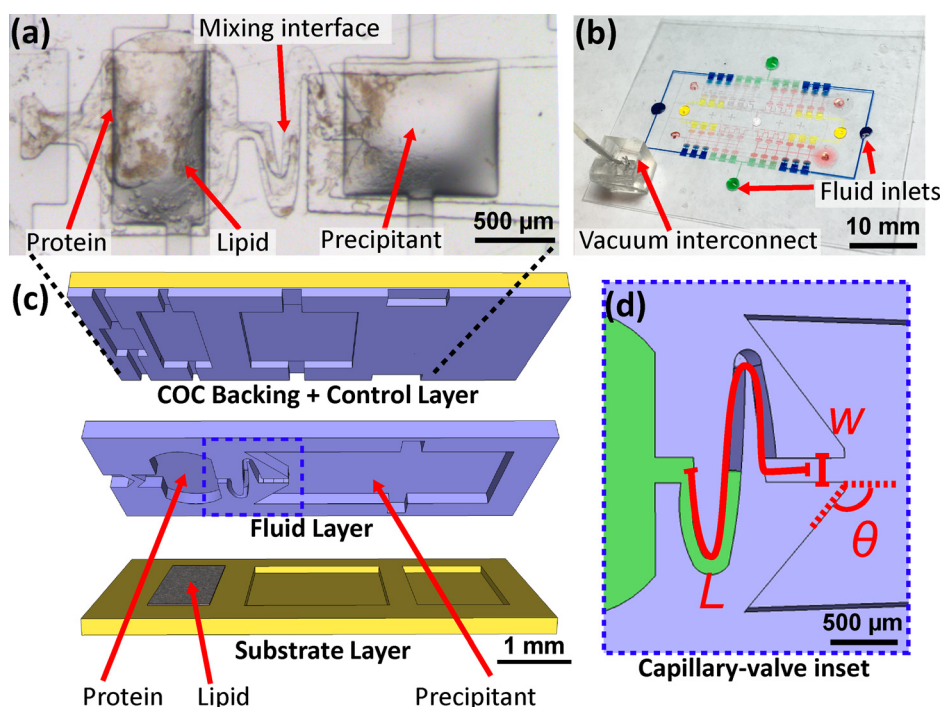
FIG. 1. Architecture of a single microfluidic *in meso* crystallization well. (a) Optical micrograph of a single crystallization well during a crystallization experiment. Protein and precipitant meet at a mixing interface in an open-ended capillary valve for passive mixing by free interface diffusion. (b) Photograph of a microfluidic array chip for *in meso* crystallization, showing a chip filled with protein (red solution) and precipitants (blue, green, yellow, and clear solutions). (c) Exploded schematic of a single crystallization well. X-ray transparency is achieved by construction with $<200\,\mu m$ of low-scattering materials. (d) Inset of the open-ended capillary valve, highlighting key optimization parameters indicated with capped red lines or red angles. Experimental studies of width ($w$), expansion angle ($\theta$), and length ($L$) resulted in an optimal valve geometry for high-throughput chips.

minutes, the mesophase and precipitant reservoir stay in contact indefinitely across the normally open capillary valve to ensure mixing to completion. A multilayer hybrid chip architecture of two polymers is required for chip functionality: (1) elastomeric polydimethylsiloxane (PDMS) for the fluid layer and control layer, which enables the use of normally closed, vacuum-actuated valves for filling and fluid routing and (2) rigid, impermeable cyclic olefin copolymer (COC), which enables long-term incubations ($>1$ month) for crystal growth. Further, the chip construction of thin PDMS layers (X-ray path length: $\sim 20\,\mu m$) sandwiched between two COC layers (X-ray path length: $\sim 75\,\mu m$) imparts the chips with X-ray transparency for *in situ* crystal diffraction experiments (Figure 1(c)).[28,30]

In contrast to prior work, this approach addresses the challenges of scale-down (volume of reagents) and scale-out (number of tests) in the design of the chip. To automate high-throughput screening, a large number of wells are needed on a single chip. To accomplish this, the footprint of each microfluidic well was scaled-down and re-designed to fit modularly in dense arrays. Features in the vacuum control layer were reconfigured compared to previous work: in these scaled-out chips, as few as 2 control lines automate filling and mixing in every well. Additionally, the filling strategy was modified to use an open-ended capillary valve to optimize handling volumes as small as 8 nl. Capillary valves are routinely employed in the field of centrifugal microfluidics,[39] but in this report, the strategy is adapted to vacuum-actuated microfluidics. The open-ended capillary valve balanced the vacuum-induced force that drives dead-end filling with resistance to flow in a narrow microfluidic channel. Test arrays that varied the width, length, and expansion angle of the open-ended capillary valve were used to determine an optimal valve geometry, and after testing, a long "S"-shaped channel resulted in the best performance (Figures 1(d) and S2 (supplementary material)).

Microfluidic arrays were built using these wells to address two challenges in membrane protein crystallization: (A) high-throughput screening for crystallization hits and (B) optimization of crystallization hits.

## B. High-throughput crystallization screening of novel membrane proteins in microfluidic arrays.

To facilitate the discovery of suitable conditions for growing diffraction-quality crystals, dense microfluidic arrays of up to 192 wells for *in meso* crystallization were designed (Figure 2(a)). These high-throughput devices mix a single membrane protein sample with up to 48 different precipitant solutions. Membrane protein solution fills through two inlets into 192 protein compartments of varying sizes. Precipitants fill through 48 inlets into sets of 4 precipitant



**(b) Ratios**

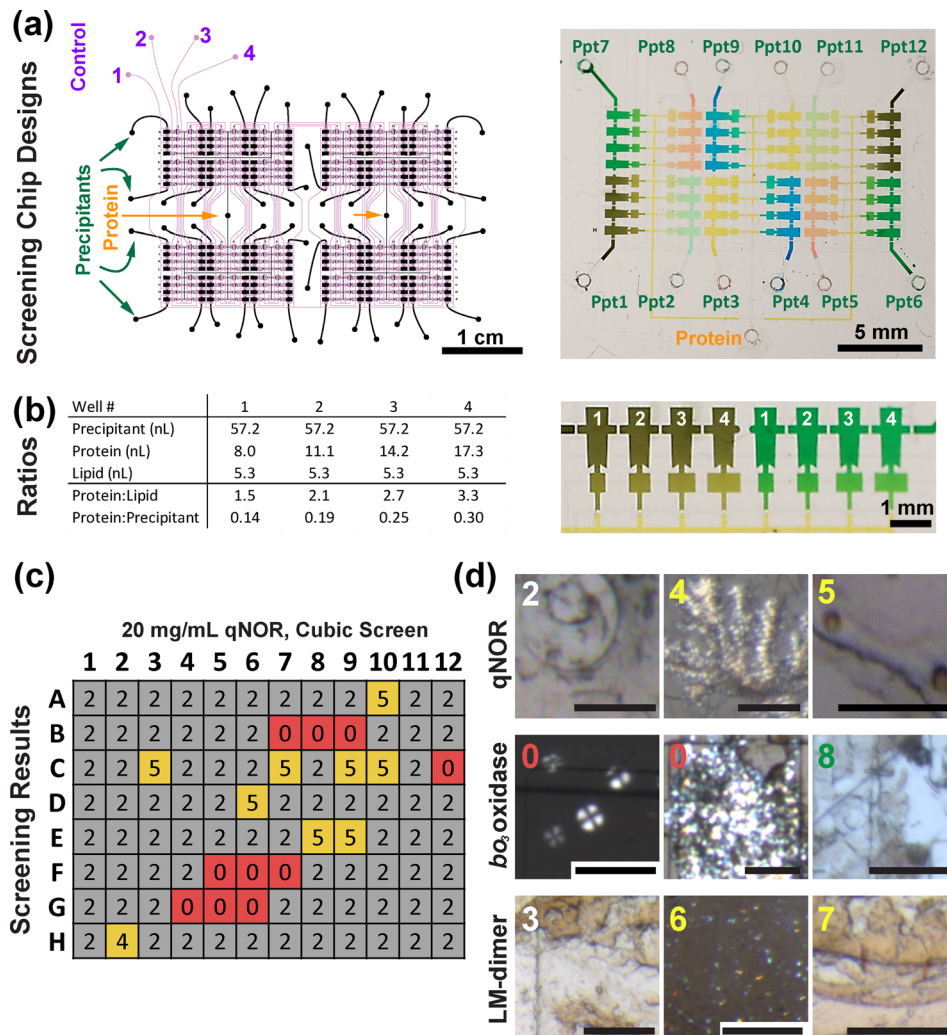| Well # | 1 | 2 | 3 | 4 |
|---|---|---|---|---|
| Precipitant (nL) | 57.2 | 57.2 | 57.2 | 57.2 |
| Protein (nL) | 8.0 | 11.1 | 14.2 | 17.3 |
| Lipid (nL) | 5.3 | 5.3 | 5.3 | 5.3 |
| Protein:Lipid | 1.5 | 2.1 | 2.7 | 3.3 |
| Protein:Precipitant | 0.14 | 0.19 | 0.25 | 0.30 |

FIG. 2. High-throughput screening chips for membrane protein crystallization. (a) Designs for 192-well (*left*) and 48-well (*right*) screening chips. Fluid introduced through protein and precipitant ports mix to generate 192 unique conditions. (b) Variable protein:lipid ratios generated in high-throughput screens. As indicated in the table, the amount of lipid for mesophase formulation remains constant while the variable size of protein compartments generates a linear gradient of protein concentrations. Each precipitant mixes with four different mesophases for extensive screening. (c) Tabulated screening results for qNOR, screened at 20 mg/ml with Cubic Screen. 96 conditions (A1–H12) were screened in high-throughput chips. Scores are indicated with colors and numbers: red (0–1) and grey (2–3) for a negative result, yellow (4–6) for optimization candidates (low quality crystals, crystallites), and green (7–9) for diffraction ready crystals (not observed in shown qNOR screen). (d) Representative crystallization screening results and scores for qNOR, cytochrome *bo₃* oxidase, and the LM-dimer (3 conditions each) as visualized on-chip with light or cross-polarized microscopy.

compartments. Prior to filling with membrane protein and precipitants, ∼5 nl of monoolein was deposited into compartments in the patterned COC substrate layer,[30] after which the TLA was aligned and reversibly sealed to complete the assembly of high-throughput chips (Figure 1(c)).

To begin a high-throughput screening experiment, 2.5 μl of membrane protein solution was pipetted onto each protein inlet. Next, vacuum actuation of control lines 3 and 4 (Figure 2(a)) initiated filling of 8–17 nl of protein solution into each protein compartment directly on top of the monoolein. After a 4 h incubation to allow protein–lipid mixing by passive diffusion, 1 μl each of the 48 different precipitant solutions were pipetted onto the precipitant inlets. Vacuum actuation of control lines 1 and 2 initiated filling of precipitants into each precipitant compartment. Chips were incubated for up to 8 weeks and regularly monitored for crystallization with polarized light microscopy. As previously discussed, the protein-to-lipid ratio (2:3 in coupled syringes, 2:1 for passive mixing) used traditionally in screening is derived from a binary mono-olein–water phase diagram, the behavior of which may significantly change upon addition of salts, detergents, and precipitants. On microfluidic chips, mesophase mixing occurs independently in each well. To enhance and widen the extent of screening, chips are designed to vary the protein-to-lipid ratio from one well to the next based on the size of the protein compartment. In contrast to off-chip work where mesophases are usually prepared in bulk with coupled-syringes and to prior on-chip work where protein-to-lipid ratio was maintained at 2:1, high-throughput chips screen protein-to-lipid ratios from 1.5:1 to 3.3:1 for each precipitant (Figure 2(b)). To screen the same conditions via passive mixing *in meso* crystallization in a well plate (with pre-deposited lipid), 284 individual pipetting actions would be required, while the microfluidic approach presented here both conserves protein sample and reduces the burden on the experimenter by requiring 50 pipetting actions.

To validate the screening capabilities of these high-throughput microfluidic chips, three membrane proteins that were not previously crystallized *in meso* were screened: (1) quinol nitric oxide reductase (qNOR) from *Persephonella marina*, (2) cytochrome $bo_3$ oxidase from *Escherichia coli*, and (3) the LM-dimer of reaction center from *Rhodobacter sphaeroides*. Protein concentrations ranged from 5–20 mg/ml for each of the proteins. Precipitants from an *in meso* compatible screening kit, Cubic Screen (Emerald Bioscience), were used.[40] Chips were observed with optical and cross-polarized microscopy at scheduled intervals after the chips were set-up. Each well was evaluated and assigned a score using an *in meso* crystallization scoring system:[21] scores from 0–1 indicated incompatibility with the mesophase, 2–3 indicated no notable crystal hit, 4–6 indicated a hit that may lead to crystals upon optimization, and 7–9 indicated crystal growth. For each protein, on-chip screening was conducted at variable protein concentrations and variable precipitant concentrations. Extended experimental details are included in the supplementary material.

For some protein–detergent combinations, high concentration samples prepared in centrifugal concentrators resulted in a persistent bulk birefringent phase when observed through crossed polarizers. Birefringence indicates that a stable cubic phase has not formed, and the likelihood of crystallization is low. In the previous literature, high detergent concentrations have been shown to destabilize cubic phases.[41] This is particularly prevalent with some detergents commonly used in crystallization, including DDM and OG, which were used in this study to stabilize qNOR and cytochrome $bo_3$ oxidase, as they either form large protein–detergent complexes that not pass through a centrifugal concentrator or as they have a high critical micelle concentration.[42] Passive mixing approaches facilitate screening with lower protein concentrations due to a concentrating effect during the mixing process.[19] Compared to initial screens, reduced concentrations (qNOR: <10 mg/ml, cytochrome $bo_3$ oxidase: <15 mg/ml) yielded stable cubic phases and successful crystallization screening. Several crystallization hits were successfully identified for the target proteins within 14 d, and representative results and screening data are shown in Figures 2(c) and 2(d) (Table S1 of the supplementary material).

Next, diffraction quality of the hits discovered for each membrane protein was evaluated. Screening chips were directly mounted without modifying the goniometer at beamlines 21-ID-D or 23-ID-B for room-temperature X-ray diffraction experiments. To accomplish this, a magnetic cap mount was modified with a tube with a thin slit and a set-screw to hold the

microfluidic chips. Crystal hits were identified and targeted via an on-axis video microscope and sequentially probed with X-rays: (1) qNOR crystal hits yielded either no diffraction or weak scattering rings, (2) cytochrome *bo₃* oxidase crystal hits yielded weak, low resolution diffraction ($<12\,\text{Å}$), and (3) LM-dimer crystal hits yielded no identifiable diffraction. Unfortunately, optimization of these hits did not yield crystals with better diffraction, indicating that either (a) a wider range of chemical compositions must be evaluated to uncover "good" crystallization hits or (b) these proteins or particular protein preparations (choice of buffer, detergents, and additives) are intractable and resistant to forming high-quality crystals. A more complex crystallization device could broaden the variety of crystallization conditions screened in parallel by either sampling more precipitant-to-mesophase ratios or introducing on-chip serial dilutions[43] to screen a fine-gradient of concentrations for each precipitant. Regardless, through successfully screening crystallization conditions, identifying new hits, and evaluating their diffraction with X-rays, this work demonstrates an automated high-throughput *in situ* approach for *in meso* crystallization screening with minimal sample consumption.

## C. Crystallization hit optimization in combinatorial mixing chips

Microfluidic optimization chips were developed to facilitate the optimization of poorly diffracting crystallization screening hits. These experiments sample a fine-gradient of protein and precipitant mixtures, based on the condition obtained in the initial trial, in fully combinatorial 48-well arrays. On a single chip, 4 concentration or composition variants of a protein solution are mixed with 4 variants of a precipitant solution in all possible combinations. Four inlets for protein solution (P1–P4) fill the protein compartments in each of the 4 quadrants of the chip, while 7 inlets for precipitant solutions fill the precipitant compartments (4 unique solutions, Ppt1–Ppt4) and formulate 16 unique combinations of *in meso* crystallization conditions in triplicate (Figure 3(a)).

The parameters to be optimized (e.g., protein concentration, pH, precipitant concentration, and additive concentration) are chosen and prepared off-chip. The operation of the chip is similar to the operation of high-throughput screening chips with a few small differences. To begin an optimization experiment, first 1 $\mu$l of each protein solution was pipetted onto each of the protein inlets. Next, actuation of control line 2 initiated filling of protein into the protein compartment directly on top of the lipid. After a 4 h incubation to allow protein–lipid mixing by passive diffusion, 1 $\mu$l of each of the 4 precipitant variants were pipetted onto their respective inlets (Figure 3(a)). Actuation of control line 1 initiated the filling of precipitant into each precipitant compartment. To perform the same optimization experiment for passive mixing *in meso* crystallization in a well plate (with pre-deposited lipid), 96 individual pipetting actions would be required, while the microfluidic approach presented here requires just 11 pipetting actions.

Two proteins were used for testing and validating these optimization chips: a microbial rhodopsin from *Haloquadratum walsbyi* and a photosynthetic reaction center mutant from *Rhodobacter sphaeroides*, denoted L223SW. Initial testing of crystallization and fluid flow for the optimization device were conducted with microbial rhodopsin, a photochemically active seven-transmembrane $\alpha$-helical protein with a covalently bound retinal chromophore. Microbial rhodopsin crystals appeared on-chip after 4 weeks of incubation with known crystallization conditions (7.5 mg/ml in 50 mM MES pH 6.5, 500 mM NaCl, 1% OG mixed with 7%–10% Tacsimate pH 7, 20% PEG 3350).[44] X-ray diffraction data were collected, but these crystals rapidly lost color and showed reduction in diffraction quality upon exposure to light and X-rays (Figure S3 of the supplementary material). Due to the lengthy crystallization time and fragility of microbial rhodopsin crystals, validation experiments were instead carried out with the L223SW mutant. The L223SW mutant was designed for fundamental structure–function experiments to study the mechanism of electron transport in photosynthetic reaction centers. The crystal structure and crystallization conditions are known for the wild-type protein, and we previously grew crystals on chip and solved the structure for the wild-type reaction center (PDB: 4TQQ).[30] As a starting point, crystallization was attempted with the condition used in prior work (15 mg/ml reaction center in 10 mM Tris pH 7.8, 280 mM NaCl, 0.05%
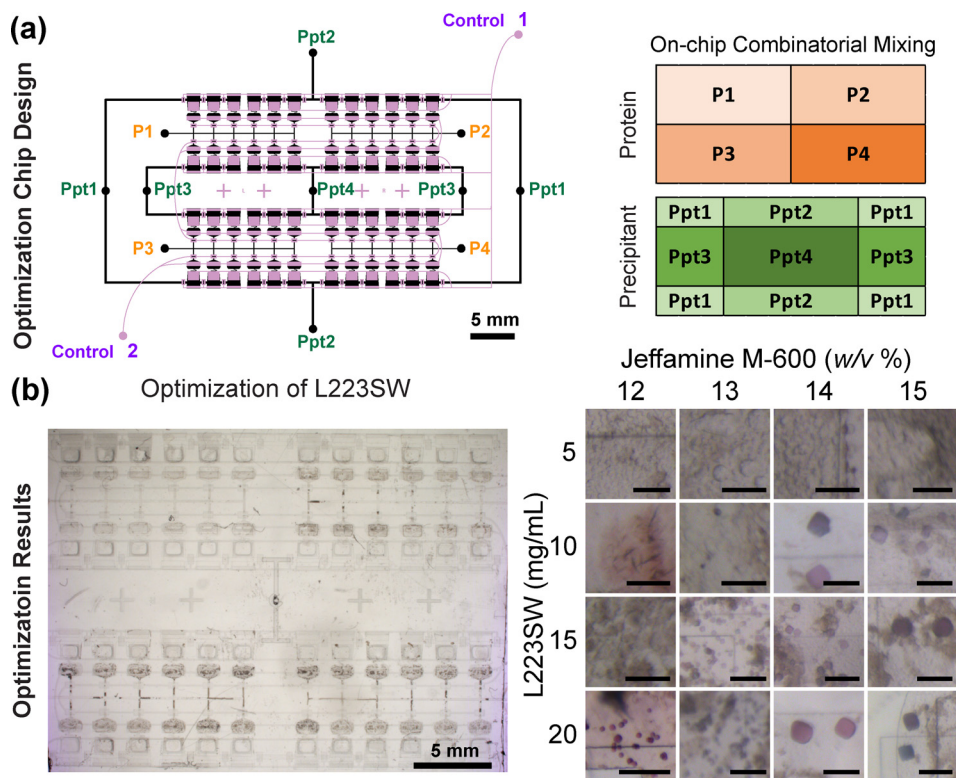
FIG. 3. Optimization chips for membrane protein crystallization. (a) Design of a 48-well chip (*left*) and fluid filling scheme (*right*) for a crystallization optimization experiment. The mixing array formulates fully combinatorial *in meso* crystallization experiments for 4 different levels of both protein and precipitant, aiding the search for diffraction-quality crystals once proper precipitant components are discovered via screening. (b) (*left*) Photograph of on-chip optimization experiment for L223SW observed 10d after set-up. (*right*) Representative optimization results from each condition formulated on a single chip. No crystallization was observed at low protein concentration, and many small crystals appeared at high protein concentration and low precipitant concentration. The best crystals were observed at higher protein concentrations (15 and 20 mg/ml) and high precipitant concentrations (14%–15%). Scale bars: 100 $\mu$m

Lauryldimethylamine oxide (LDAO) mixed with 1 M HEPES, 1.15 M $(NH_4)_2SO_4$, 13% *w/v* Jeffamine M-600 adjusted to pH 7.5). However, this condition produced small crystals with L223SW that diffracted only to 6 Å, while the wild-type crystals had diffracted to 2.5 Å. To obtain structure-quality crystallization conditions for L223SW, changes in protein concentration, pH, and precipitant concentration were analyzed with optimization chips (Figures 3(b) and S4 (supplementary material)). Changes in pH either had a negative or no effect on crystallization. High concentrations of protein and low concentrations of precipitant resulted in small ($\sim$20 $\mu$m), poorly diffracting ($\sim$6 Å) crystals, while high concentrations of both protein and precipitant solutions resulted in the largest crystals ($\sim$60 $\mu$m) with good diffraction ($\sim$3.2 Å). The best diffracting crystals were grown with 20 mg/ml protein at pH 7.8 using high concentrations of Jeffamine M-600 (14%–15% *w/v*).

Following a previously developed on-chip data collection strategy for room-temperature crystals,[30] *in situ* data were collected from multiple crystals in small wedges and then merged together to minimize the effect of radiation damage on the structure. In total, 19 crystals from a small range of conditions (15–20 mg/ml for protein, 14%–15% *w/v* Jeffamine M-600) were selected to form an optimal dataset. Despite the small variations in chemical composition, the crystals had near identical lattice parameters ($<$0.5% variation) and a small variation in mosaicity. Interestingly, crystallization at 20 mg/ml L223SW and 15% *w/v* Jeffamine M-600 yielded the lowest mosaicity crystals and also the highest quality of diffraction (3.2 Å). The crystal structure of L223SW was solved to a resolution of 3.5 Å (Figure S5, Table S2 (supplementary material), PDB: 5V33). In the wild-type protein, a serine located in the L-subunit at position 223 facilitates the binding of a quinone ($Q_B$) molecule, which serves as the terminal electron
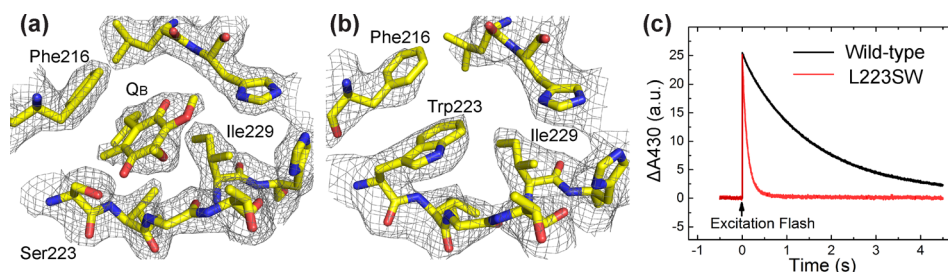
FIG. 4. The secondary quinone ($Q_B$) binding pocket in the L-subunit of *R. sphaeroides* reaction center. (a) The binding pocket in the wild-type structure where $Q_B$, a ubiquinone-8 molecule that serves as the terminal electron acceptor, is present. (b) The $Q_B$ binding pocket in the L223SW mutant, where the mutated residue (serine to tryptophan) blocks the binding pocket, inhibiting the binding of $Q_B$. All $2F_O$–$F_c$ maps are contoured to $\pm 1\sigma$. (c) Flash-induced spectroscopy of wild-type and mutant reaction centers. In the wild-type where $Q_B$ is present, the backward electron transfer from $Q_B^-$ to the special pair of bacteriochlorophyll $P^+$ has a lifetime of ∼1 s. In contrast, in the mutant where $Q_B$ is absent, the electron transfer from $Q_A^-$ to $P^+$ has a lifetime of ∼0.1 s. This spectroscopic measurement indicates that a functional $Q_B$ is absent in the L223SW mutant.

acceptor for the reaction center. Both residue Ser223 and $Q_B$ are resolved in the wild-type crystal structure (Figure 4(a)). In the mutant protein, the small polar residue Ser223 is replaced with tryptophan, a relatively large hydrophobic residue (Trp223, also denoted S223W). In the solved structure, Trp223 protrudes into the binding pocket, which prevents $Q_B$ from binding (Figure 4(b)). This structural observation matches observations from flash-induced spectroscopy: with a $Q_B$ present in the wild-type protein, electron transfer has a lifetime of about 1 s, whereas, when $Q_B$ is absent in the mutant, electron transfer has a lifetime of about 100 ms (Figure 4(c)). Previous studies that used a molecular additive to inhibit charge transfer from $Q_A$ to $Q_B$ observed a 10-fold reduction in lifetime of the charge-separated state, agreeing with this structural and spectroscopic observation.[45] Through successfully optimizing the diffraction quality of crystals, this work demonstrates the application of microfluidic optimization chips as effective tools for streamlining crystallography and for supporting structure–function studies that require atomic-resolution crystal structures.

## IV. CONCLUSIONS

In summary, X-ray transparent microfluidic devices for *in meso* crystallization screening and optimization were developed that automated the formulation of mesophases for crystallization experiments in a high-throughput manner while consuming just a few nanoliters of membrane protein solution per condition. The high-throughput screening devices were validated by discovering crystallization hits for qNOR, cytochrome *bo₃* oxidase, and the LM-dimer of reaction center. The ability to survey 192 unique crystallization conditions in parallel with an X-ray transparent platform expedites extensive screening, crystal hit identification, and diffraction testing, all without opening or altering the device. In addition, the optimization devices were validated using the crystallization of the L223SW mutant of reaction center. Starting from a condition that yielded low quality crystals, fine-gradient re-screening of L223SW led to large, diffraction quality crystals. Data from these crystals were used to resolve a room-temperature structure with a 3.5 Å resolution. Compared to the wild-type reaction center structure, the L223SW structure verified that the S223W mutation inhibits the binding of a secondary ubiquinone to reaction center. For optimum performance of both devices, simple vacuum actuation and diffusive mixing are key to facilitating device-wide filling and incubation of all wells. The open-ended capillary valve enabled these devices to precisely measure as little as 8 nl of protein solution to form a 13 nl crystallization-ready mesophase, a ∼60% decrease in sample usage when compared to the most efficient *in meso* robots.[7] While this technique is currently exclusive to laboratories with microfluidics expertise and their collaborators, the development of this technology into a commercially available product as an alternative to traditional *in meso* crystallization plates would provide immense advantages in user-friendliness and sample usage.

The precise dispensing, control over fluid routing, and X-ray transparency in this type of microfluidic device may facilitate their use for other delicate, complicated, and labor-intensive *in meso* crystallization experiments. As the field of crystallography pushes toward brighter X-ray beams and smaller crystals for serial crystallography,[46–48] high-throughput devices that can grow hundreds of crystals on the same device (as reported here) provide an excellent fixed-target platform[49–51] that has key advantages over continuous liquid-injection jets.[52–55] Further, a more advanced device could facilitate crystal soaking, i.e., the on-chip introduction of heavy atoms or anomalous scatterers[56–58] into the crystal post-crystallization for *in situ*, *de novo* phasing experiments.

## SUPPLEMENTARY MATERIAL

See supplementary material for details on device fabrication, chip operation, capillary valve testing, crystallization of microbial rhodopsin, additional screening and optimization experiments, X-ray diffraction set-up, and structural statistics.

## ACKNOWLEDGMENTS

[1] E. F. Garman, Science **343**, 1102 (2014).
[2] V. V. Lounnas, T. Ritschel, J. Kelder, R. McGuire, R. P. Bywater, and N. Foloppe, Comput. Struct. Biotechnol. J. **5**, e201302011 (2013).
[3] J. P. Overington, B. Al-Lazikani, and A. L. Hopkins, Nat. Rev. Drug Discovery **5**, 993 (2006).
[4] H. Michel, Trends Biochem Sci. **8**, 56 (1983).
[5] E. M. Landau and J. P. Rosenbusch, Proc. Natl. Acad. Sci. U.S.A. **93**, 14532 (1996).
[6] S. G. F. Rasmussen, B. T. DeVree, Y. Zou, A. C. Kruse, K. Y. Chung, T. S. Kobilka, F. S. Thian, P. S. Chae, E. Pardon, D. Calinski, J. M. Mathiesen, S. T. A. Shah, J. A. Lyons, M. Caffrey, S. H. Gellman, J. Steyaert, G. Skiniotis, W. I. Weis, R. K. Sunahara, and B. K. Kobilka, Nature **477**, 549 (2011).
[7] M. Caffrey, Acta Crystallogr., Sect. F: Struct. Biol. Commun. **71**, 3 (2015).
[8] M. Caffrey, Curr. Opin. Struct. Biol. **10**, 486 (2000).
[9] I. Moraes, G. Evans, J. Sanchez-Weatherby, S. Newstead, and P. D. S. Stewart, Biochim. Biophys. Acta **1838**, 78 (2014).
[10] N. E. Chayen, Curr. Opin. Struct. Biol. **14**, 577 (2004).
[11] N. E. Chayen and E. Saridakis, Nat. Methods **5**, 147 (2008).
[12] Y. M. Liu, H. S. Li, Z. Q. Wu, R. Q. Chen, Q. Q. Lu, Y. Z. Guo, C. Y. Zhang, and D. C. Yin, CrystEngComm **18**, 1609 (2016).
[13] R. Q. Chen, D. C. Yin, Q. Q. Lu, J. Y. Shi, and X. L. Ma, Acta Crystallogr., Sect. D: Biol. Crystallogr. **68**, 584 (2012).
[14] E. F. Garman and R. L. Owen, Acta Crystallogr., Sect. D: Biol. Crystallogr. **62**, 32 (2006).
[15] J. S. Fraser, H. van den Bedem, A. J. Samelson, P. T. Lang, J. M. Holton, N. Echols, and T. Alber, Proc. Natl. Acad. Sci. U.S.A. **108**, 16247 (2011).
[16] J. Briggs, H. Chung, and M. Caffrey, J. Phys. II **5**, 723 (1996).
[17] V. Cherezov, H. Fersi, and M. Caffrey, Biophys. J. **81**, 225 (2001).
[18] P. Wadsten, A. B. Wöhri, A. Snijder, G. Katona, A. T. Gardiner, R. J. Cogdell, R. Neutze, and S. Engström, J. Mol. Biol. **364**, 44 (2006).
[19] E. Wallace, D. Dranow, P. D. Laible, J. Christensen, and P. Nollert, PLoS One **6**, e24488 (2011).
[20] J. Kubicek, R. Schlesinger, C. Baeken, G. Büldt, F. Schäfer, and J. Labahn, PLoS One **7**, e35458 (2012).
[21] M. Caffrey and V. Cherezov, Nat. Protoc. **4**, 706 (2009).
[22] D. Li, C. Boland, K. Walsh, and M. Caffrey, J. Visualized Exp. **67**, e4000 (2012).
[23] D. Li, C. Boland, D. Aragao, K. Walsh, and M. Caffrey, J. Visualized Exp. **67**, e4001 (2012).

[24]C.-Y. Y. Huang, V. Olieric, P. Ma, E. Panepucci, K. Diederichs, M. Wang, and M. Caffrey, Acta Crystallogr., Sect. D: Biol. Crystallogr. **71**, 1238 (2015).

[25]J. Broecker, V. Klingel, W.-L. Ou, A. R. Balo, D. J. Kissick, C. M. Ogata, A. Kuo, and O. P. Ernst, Cryst. Growth Des. **16**, 6318 (2016).

[26]L. Li, Q. Fu, C. A. Kors, L. Stewart, P. Nollert, P. D. Laible, and R. F. Ismagilov, Microfluid. Nanofluid. **8**, 789 (2010).

[27]S. L. Perry, G. W. Roberts, J. D. Tice, R. B. Gennis, and P. J. A. Kenis, Cryst. Growth Des. **9**, 2566 (2009).

[28]S. Guha, S. L. Perry, A. S. Pawate, and P. J. A. Kenis, Sens. Actuators, B **174**, 1 (2012).

[29]K. Dhouib, C. K. Malek, W. Pfleging, B. Gauthier-Manuel, R. Duffait, G. Thuillier, R. Ferrigno, L. Jacquamet, J. Ohana, J.-L. Ferrer, A. Théobald-Dietrich, R. Giegé, B. Lorber, and C. Sauter, Lab Chip **9**, 1412 (2009).

[30]D. S. Khvostichenko, J. M. Schieferstein, A. S. Pawate, P. D. Laible, and P. J. A. Kenis, Cryst. Growth Des. **14**, 4886 (2014).

[31]P. R. Jaschke, R. G. Saer, S. Noll, and J. T. Beatty, *Modification of the Genome of Rhodobacter Sphaeroides and Construction of Synthetic Operons*, 1st ed. (Elsevier Inc., 2011).

[32]A. Tehrani and J. T. Beatty, Photosynth. Res. **79**, 101 (2004).

[33]C. Sun, A.-M. Carey, B. Gao, C. A. Wraight, N. W. Woodbury, and S. Lin, J. Phys. Chem. B **120**, 5395 (2016).

[34]R. J. Debus, G. Feher, and M. Y. Okamura, Biochemistry **24**, 2488 (1985).

[35]M. T. Lin, L. J. Sperling, H. L. Frericks Schmidt, M. Tang, R. I. Samoilova, T. Kumasaka, T. Iwasaki, S. A. Dikanov, C. M. Rienstra, and R. B. Gennis, Methods **55**, 370 (2011).

[36]M. A. Unger, H. P. Chou, T. Thorsen, A. Scherer, and S. R. Quake, Science **288**, 113 (2000).

[37]Z. Otwinowski and W. Minor, Methods Enzymol. **276**, 307 (1997).

[38]P. D. Adams, P. V. Afonine, G. Bunkóczi, V. B. Chen, I. W. Davis, N. Echols, J. J. Headd, L. W. Hung, G. J. Kapral, R. W. Grosse-Kunstleve, A. J. McCoy, N. W. Moriarty, R. Oeffner, R. J. Read, D. C. Richardson, J. S. Richardson, T. C. Terwilliger, and P. H. Zwart, Acta Crystallogr. Sect. D: Biol. Crystallogr. **66**, 213 (2010).

[39]J. L. Moore, A. McCuiston, I. Mittendorf, R. Ottway, and R. D. Johnson, Microfluid. Nanofluid. **10**, 877 (2011).

[40]L. van't Hag, C. Darmanin, T. C. Le, S. Mudie, C. E. Conn, and C. J. Drummond, Cryst. Growth Des. **14**, 1771–1781 (2014).

[41]Y. Misquitta and M. Caffrey, Biophys. J. **85**, 3084 (2003).

[42]P. Strop and A. T. Brunger, Protein Sci. **14**, 2207 (2005).

[43]N. L. Jeon, S. K. W. Dertinger, D. T. Chiu, I. S. Choi, A. D. Stroock, and G. Whitesides, Langmuir **16**, 8311 (2000).

[44]J. Broecker, B. T. Eger, and O. P. Ernst, Structure **25**, 384 (2017).

[45]U. Andréasson and L.-E. Andréasson, Photosynth. Res. **75**, 223 (2003).

[46]I. Schlichting, IUCrJ **2**, 246 (2015).

[47]W. Liu, D. Wacker, C. Gati, G. W. Han, D. James, D. Wang, G. Nelson, U. Weierstall, V. Katritch, A. Barty, N. A. Zatsepin, D. Li, M. Messerschmidt, S. Boutet, G. J. Williams, J. E. Koglin, M. M. Seibert, C. Wang, S. T. A. Shah, S. Basu, R. Fromme, C. Kupitz, K. N. Rendek, I. Grotjohann, P. Fromme, R. A. Kirian, K. R. Beyerlein, T. A. White, H. N. Chapman, M. Caffrey, J. C. H. Spence, R. C. Stevens, and V. Cherezov, Science **342**, 1521 (2013).

[48]P. Nogly, D. James, D. Wang, T. A. White, N. Zatsepin, A. Shilova, G. Nelson, H. Liu, L. Johansson, M. Heymann, K. Jaeger, M. Metz, C. Wickstrand, W. Wu, P. Båth, P. Berntsen, D. Oberthuer, V. Panneels, V. Cherezov, H. Chapman, G. Schertler, R. Neutze, J. Spence, I. Moraes, M. Burghammer, J. Standfuss, and U. Weierstall, IUCrJ **2**, 168 (2015).

[49]M. S. Hunter, B. Segelke, M. Messerschmidt, G. J. Williams, N. A. Zatsepin, A. Barty, W. H. Benner, D. B. Carlson, M. Coleman, A. Graf, S. P. Hau-Riege, T. Pardini, M. M. Seibert, J. Evans, S. Boutet, and M. Frank, Sci. Rep. **4**, 6026 (2014).

[50]G. K. Feld, M. Heymann, W. H. Benner, T. Pardini, C.-J. Tsai, S. Boutet, M. A. Coleman, M. S. Hunter, X. Li, M. Messerschmidt, A. Opthalage, B. Pedrini, G. J. Williams, B. A. Krantz, S. Fraden, S. Hau-Riege, J. E. Evans, B. W. Segelke, and M. Frank, J. Appl. Crystallogr. **48**, 1072 (2015).

[51]C. Mueller, A. Marx, S. W. Epp, Y. Zhong, A. Kuo, A. R. Balo, J. Soman, F. Schotte, H. T. Lemke, R. L. Owen, E. F. Pai, A. R. Pearson, J. S. Olson, P. A. Anfinrud, O. P. Ernst, and R. J. D. Miller, Struct. Dyn. (Melville, N.Y.) **2**, 54302 (2015).

[52]U. Weierstall, Philos Trans R. Soc. B: Biol. Sci. **369**, 20130337 (2014).

[53]P. Nogly, V. Panneels, G. Nelson, C. Gati, T. Kimura, C. Milne, D. Milathianaki, M. Kubo, W. Wu, C. Conrad, J. Coe, R. Bean, Y. Zhao, P. Båth, R. Dods, R. Harimoorthy, K. R. Beyerlein, J. Rheinberger, D. James, D. DePonte, C. Li, L. Sala, G. J. Williams, M. S. Hunter, J. E. Koglin, P. Berntsen, E. Nango, S. Iwata, H. N. Chapman, P. Fromme, M. Frank, R. Abela, S. Boutet, A. Barty, T. A. White, U. Weierstall, J. Spence, R. Neutze, G. Schertler, and J. Standfuss, Nat. Commun. **7**, 12314 (2016).

[54]U. Weierstall, D. James, C. Wang, T. A. White, D. Wang, W. Liu, J. C. H. Spence, R. Bruce Doak, G. Nelson, P. Fromme, R. Fromme, I. Grotjohann, C. Kupitz, N. A. Zatsepin, H. Liu, S. Basu, D. Wacker, G. W. Han, V. Katritch, S. Boutet, M. Messerschmidt, G. J. Williams, J. E. Koglin, M. M. Seibert, M. Klinker, C. Gati, R. L. Shoeman, A. Barty, H. N. Chapman, R. A. Kirian, K. R. Beyerlein, R. C. Stevens, D. Li, S. T. A. Shah, N. Howe, M. Caffrey, and V. Cherezov, Nat. Commun. **5**, 3309 (2014).

[55]W. Liu, A. Ishchenko, and V. Cherezov, Nat. Protoc. **9**, 2123 (2014).

[56]W. A. Hendrickson, Science **254**, 51 (1991).

[57]A. C. W. Pike, E. F. Garman, T. Krojer, F. von Delft, and E. P. Carpenter, Acta Crystallogr., Sect. D: Struct. Biol. **72**, 303 (2016).

[58]D. Li, V. E. Pye, and M. Caffrey, Acta Crystallogr., Sect. D: Biol. Crystallogr. **71**, 104 (2015).